

An analytic model for non-spherical lenses in covariant MOND

HuanYuan Shan^{1*}, Martin Feix^{2*}, Benoit Famaey³ and HongSheng Zhao^{2,1}

¹National Astronomical Observatories, Chinese Academy of Sciences, 20A Datun Road, Chaoyang District, 100012, Beijing, China

²SUPA, School of Physics and Astronomy, University of St Andrews, North Haugh, St Andrews, Fife, KY16 9SS, United Kingdom

³Institut d’Astronomie et d’Astrophysique, Université Libre de Bruxelles, CP226, Bvd du Triomphe, B-1050, Bruxelles, Belgium

Accepted Received . . . ; in original form . . .

ABSTRACT

Strong gravitational lensing by galaxies in modified Newtonian dynamics (MOND) has until now been restricted to spherically symmetric models. These models were able to account for the size of the Einstein ring of observed lenses, but were unable to account for double-imaged systems with collinear images, as well as four-image lenses. Non-spherical models are generally cumbersome to compute numerically in MOND, but we present here a class of analytic non-spherical models that can be applied to fit double-imaged and quadruple-imaged systems. We use them to obtain a reasonable MOND fit to ten double-imaged systems, as well as to the quadruple-imaged system Q2237+030 which is an isolated bulge-disk lens producing an Einstein cross. However, we also find five double-imaged systems and three quadruple-imaged systems for which no reasonable MOND fit can be obtained with our models. We argue that this is mostly due to the intrinsic limitation of the analytic models, even though the presence of small amounts of additional dark mass on galaxy scales in MOND is also plausible.

Key words: cosmology: theory - gravity - dark matter - gravitational lensing

1 INTRODUCTION

The modified Newtonian dynamics paradigm (MOND, Milgrom 1983) has been originally proposed as an alternative to galactic (cold) dark matter (CDM). This paradigm postulates a modification of Newton’s laws in order to explain the rotation curves of spiral galaxies, by saying that the MONDian gravitational accelerations $g_M \ll a_0 \approx 10^{-10} \text{ m s}^{-2}$ approach $(g_N a_0)^{1/2}$ where g_N is the usual Newtonian gravitational acceleration. Nowadays, this paradigm is still better suited than dark matter to explain the observed conspiracy between the distribution of baryons and the gravitational field in spiral galaxies (e.g., McGaugh et al. 2007; Famaey et al. 2007c). Indeed, it is baffling that such a simple prescription leads to uncannily successful predictions for galaxies ranging over five decades in mass (see, e.g., Sanders & McGaugh 2002; Bekenstein 2006 for reviews), including our own Milky Way (Famaey & Binney 2005; Famaey et al. 2007b).

On the other hand, recent developments in the theory of gravity have also added plausibility to the case for MOND through the advent of Lorentz-covariant theories yielding this behavior in the ultra-weak gravity limit by means of a dynamical (not necessarily) normalized four-vector field (Bekenstein 2004; Zlosnik et al. 2007; Bruneton & Esposito-Farese 2007; Zhao 2007; Sanders 2005; Skordis 2008). Although rather fine-tuned and still being a far cry from a fundamental theory underpinning the MOND paradigm, these new theories remarkably al-

low for new predictions regarding cosmology (e.g., Skordis et al. 2006; Dodelson & Liguori 2006; Schmidt et al. 2007; Zhang et al. 2007) and gravitational lensing (e.g., Chiu et al. 2006; Qin et al. 1995; Zhao et al. 2006; Angus et al. 2007b; Famaey et al. 2007a; Takahashi & Chiba 2007; Xu et al. 2007).

In these Lorentz-covariant theories, gravitational lensing has actually been shown to work exactly in the same manner as in general relativity (GR) for static systems (e.g., Bekenstein 2004), except for the relation between the density and the gravitational potential. This allowed, for instance, Zhao et al. (2006) to test MOND against the CASTLES data of image-splitting lenses, building on the earlier work of Qin et al. (1995). They were nevertheless restricted to models of *spherical geometry*, and were thus only able to account for the size of the Einstein ring of observed lenses, but not for the exact position of collinear images in double-imaged systems, and of course not for quadruple-imaged systems. This intrinsic limitation is due to the fact that the MONDian acceleration \vec{g}_M is related to the Newtonian one, $\vec{g}_N = -\vec{\nabla}\Phi_N$, by (Bekenstein & Milgrom 1984)

$$\mu\left(\frac{|\vec{g}_M|}{a_0}\right)\vec{g}_M = -\vec{\nabla}\Phi_N + \vec{S}, \quad (1)$$

where \vec{S} is a solenoidal vector field determined by the condition that \vec{g}_M can be expressed as the gradient of a scalar potential Φ_M . The function μ , controlling the modification of Newton’s law, has

* E-mail: shanhuan@bao.ac.cn (HYS); mf256@st-andrews.ac.uk (MF)

the following asymptotic behavior:

$$\begin{aligned}\mu(x) &\sim x & x \ll 1, \\ \mu(x) &\sim 1 & x \gg 1.\end{aligned}\quad (2)$$

The field \vec{S} is typically non-zero in non-spherical geometry, and calculating it usually requires the use of a numerical solver for the non-linear field equation of MOND (e.g., Ciotti et al. 2006; Tiret & Combes 2007; Feix et al. 2008).

In this paper, we will demonstrate how to create simple analytic models of *non-spherical lenses* with $\vec{S} = \vec{0}$ in MOND, choosing the covariant framework of tensor-vector-scalar gravity (TeVeS, Bekenstein 2004). Without resorting to a numerical Poisson solver, these analytic models can thus be used to fit image positions in double-imaged and quadrupled-image systems. We present our analytic models in Sect. 2, devise a fitting procedure in Sect. 3, and finally expose and discuss the results in Sects. 4 and 5.

2 THE HERNQUIST-KUZMIN MODEL

2.1 Potential-density pair

The Kuzmin disk (Kuzmin 1956), defined by a Newtonian gravitational potential of the form

$$\Phi_{N,K} = \frac{-GM}{\sqrt{x^2 + y^2 + (|z| + b)^2}}, \quad b > 0 \quad (3)$$

is a well-known non-spherical case which satisfies $\vec{S} = \vec{0}$ in Eq. (1): For $z > 0$, Eq. (3) corresponds to the Newtonian potential generated by a point mass located at $(0, 0, -b)$, in case of $z < 0$ it turns into the Newtonian potential of a point mass located at $(0, 0, b)$. Thus, above and below the disk, we effectively have a spherical Newtonian potential, which implies that truly $\vec{S} = \vec{0}$ in Eq. (1).

Hereafter, the idea is simply to model lens galaxies by replacing the auxiliary point lens potential of the Kuzmin disk with an auxiliary Hernquist lens potential (Hernquist 1990); we shall refer to this model as the Hernquist-Kuzmin (HK) model. A similar approach, using Plummer's model and a smooth transition at $z = 0$ instead, leads to the Plummer-Kuzmin model derived by Miyamoto & Nagai (1975) which provides a qualitatively good fit to the mass profile of observed galaxies. Although our proposed model is not a very good description of real galaxies, it enables us to derive fully analytic lens models in the context of MOND (see Sect. 2.2) and to study the influence of non-sphericity on the ability to fit image positions.

The Newtonian potential of the Hernquist-Kuzmin model takes the form

$$\Phi_{N,HK} = \frac{-GM}{\sqrt{x^2 + y^2 + (|z| + b)^2 + h}}, \quad (4)$$

with b being the Kuzmin parameter and h denoting the core radius of the Hernquist profile. Choosing different ratios h/b , this model will produce different Hubble type galaxies, going from a pure Kuzmin disk galaxy for $h/b \rightarrow 0$ to a pure Hernquist sphere for $h/b \rightarrow \infty$. To clarify this situation and to characterize the non-sphericity of the model, one may simply expand the r.h.s of Eq. (4) far away from the disk ($r^2 = x^2 + y^2 + z^2$):

$$\Phi_{N,HK} = \frac{-GM}{r+h} \left(1 - \frac{|z|b}{(r+h)r} \right) + \mathcal{O}(b^2) \quad (5)$$

Using Poisson's equation, we find that the underlying density

distribution is given by ($R^2 = x^2 + y^2$)

$$\rho_{HK} = \frac{Mh}{2\pi \sqrt{R^2 + (|z| + b)^2} \left(\sqrt{R^2 + (|z| + b)^2 + h} \right)^3}. \quad (6)$$

The corresponding density contours in the (R, z) plane are plotted in Fig. 1 for different values of h/b .

Considering the Hernquist-Kuzmin model for gravitational lensing, we choose the z -axis such that it is parallel to the line-of-sight and x, y are the Cartesian coordinates spanning the lens plane. Because we need to account for different possible orientations of galaxies, we additionally have to rotate the disk. Defining $(r')^2 = (x')^2 + (y')^2 + (|z'| + b)^2$, where

$$\begin{aligned}x' &= (x \cos \phi - y \sin \phi) \cos \theta - z \sin \theta, \\ y' &= x \sin \phi + y \cos \phi, \\ z' &= (x \cos \phi - y \sin \phi) \sin \theta + z \cos \theta,\end{aligned}\quad (7)$$

the angle $(\pi/2) - \theta$ being the inclination of the galaxy's symmetry plane w.r.t. the line of sight and ϕ the galaxy's position angle (PA), Eq. (4) turns into

$$\Phi_{N,HK} = \frac{-GM}{r' + h}. \quad (8)$$

2.2 Lensing Properties

In this work, we consider MOND within the framework of TeVeS (Bekenstein 2004), henceforth using units with $c = 1$. Since most of the light bending still occurs within a small range around the lens compared to the distances between lens and source and observer and source, gravitational lensing works exactly the same way as in GR if the Newtonian potential is substituted by the total non-relativistic modified potential.

Then, according to Schneider et al. (1992), the resulting deflection angle can be written as

$$\vec{\alpha} = 2 \int_{-\infty}^{\infty} \vec{\nabla}_{\perp} \Phi dz, \quad (9)$$

where Φ is the total gravitational potential, $\vec{\nabla}_{\perp}$ denotes the two-dimensional gradient operator perpendicular to light propagation and integration is performed along the unperturbed light path (Born's approximation). Positions in the source and the lens plane are related through the lens equation:

$$\vec{\eta} = \frac{D_s}{D_l} \vec{\xi} - D_{ls} \vec{\alpha}(\vec{\xi}). \quad (10)$$

Here $\vec{\xi} = (x, y)$, $\vec{\eta}$ is the 2-dimensional position vector in the source plane, and D_s , D_l , and D_{ls} are the (angular diameter) distances between source and observer, lens and observer, and lens and source, respectively. Furthermore, it is convenient to introduce the deflection potential $\Psi(\vec{\theta})$:

$$\Psi(\vec{\theta}) = 2D \int \Phi(D_l \vec{\theta}, z) dz, \quad (11)$$

where we have used $\vec{\theta} = \vec{\xi}/D_l$ and $D = D_{ls}/(D_s D_l)$. If a source is much smaller than the angular scale on which the lens properties change, the lens mapping can locally be linearized. Thus, the distortion of an image can be described by the Jacobian matrix

$$\mathcal{A}(\vec{\theta}) = \frac{\partial \vec{\beta}}{\partial \vec{\theta}} = \begin{pmatrix} 1 - \kappa - \gamma_1 & -\gamma_2 \\ -\gamma_2 & 1 - \kappa + \gamma_1 \end{pmatrix}, \quad (12)$$

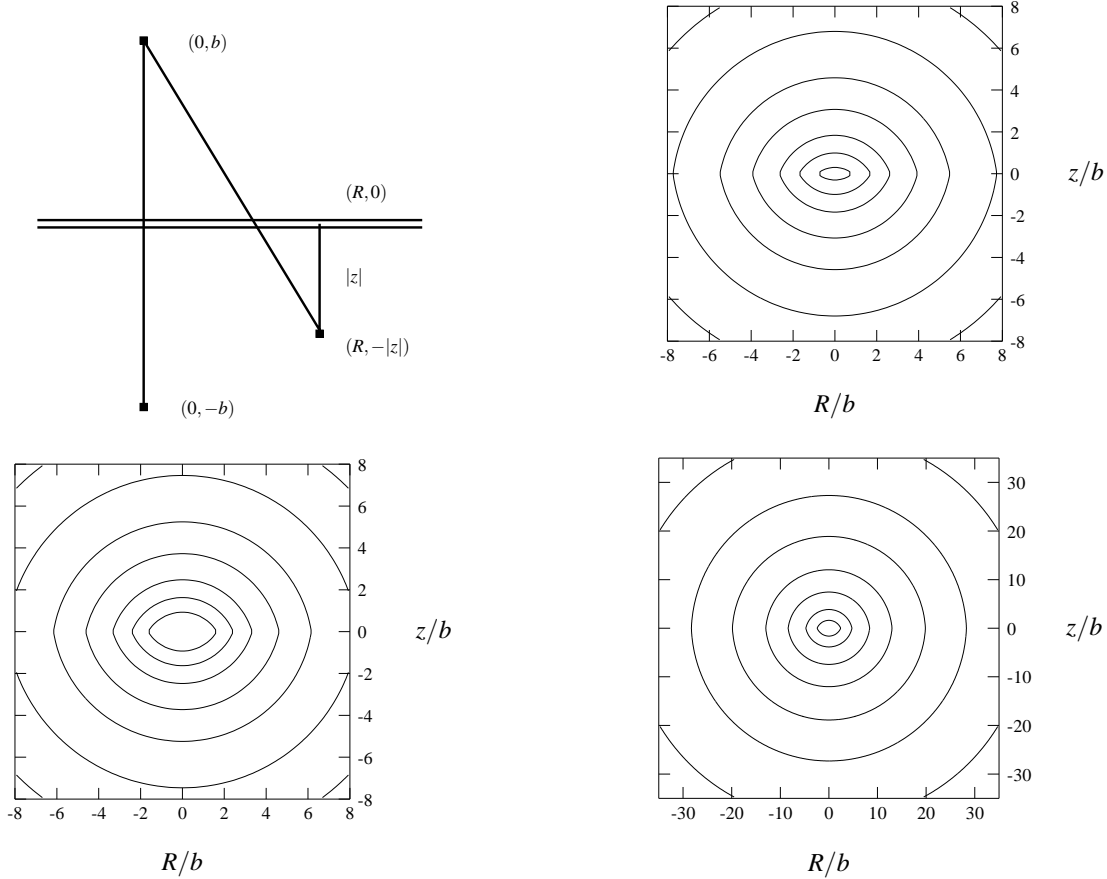


Figure 1. Contours of equal density in the (R, z) plane for the HK model (6) when $h/b = 0.1$ (top right), $h/b = 1$ (bottom left) and $h/b = 10$ (bottom right). Contour levels are $(0.01, 0.003, 0.001, \dots)M/b^3$ (top right); $(0.001, \dots)M/b^3$ (bottom left); $(0.0003, \dots)M/b^3$ (bottom right). The top left panel illustrates the HK model: At the point $(R, -|z|)$ below the disk, the potential Eq. (4) is identical with that of a Hernquist distribution whose origin is located at a distance b above the disk's center.

with the angular coordinate $\vec{\beta} = \vec{r}/D_s$. The convergence κ is directly given by the deflection potential Ψ :

$$\kappa = \frac{1}{2} \Delta_{\vec{\theta}} \Psi. \quad (13)$$

Similarly, the shear components γ_1, γ_2 can be calculated from

$$\gamma_1 = \frac{1}{2} \left(\frac{\partial^2 \Psi}{\partial \theta_1^2} - \frac{\partial^2 \Psi}{\partial \theta_2^2} \right), \quad \gamma_2 = \frac{\partial^2 \Psi}{\partial \theta_1 \partial \theta_2}, \quad (14)$$

$$\gamma = \sqrt{\gamma_1^2 + \gamma_2^2}.$$

Due to Liouville's theorem, gravitational lensing preserves the surface brightness, but it changes the apparent solid angle of a source. The resulting flux ratio between image and source can be expressed in terms of the amplification A ,

$$A^{-1} = (1 - \kappa)^2 - \gamma^2. \quad (15)$$

Consequently, the flux ratio between two images A and B is $f_{AB} = A_A/A_B$. Points in the lens plane where $A^{-1} = 0$ form closed curves, the critical curves. Their corresponding curves located in the source plane are called caustics. Images near critical curves can significantly be magnified and distorted, which, for instance, is indicated by the giant luminous arcs formed from source galaxies near caustics.

Due to the deflection by the gravitational potential, light rays traveling from a source to an observer at redshift $z = 0$ will be

delayed in time:

$$t(\vec{\theta}) = \frac{1 + z_l}{D} \left(\frac{1}{2} (\vec{\theta} - \vec{\beta})^2 - \Psi(\vec{\theta}) \right), \quad (16)$$

where z_l is the lens' redshift. If the deflection potential is known, Eq. (16) allows to calculate the relative time delay between different images.

Choosing a certain smooth transition from Newtonian dynamics to MOND (see Zhao et al. 2006, Sect. 8.2 for details) and assuming spherical symmetry, we have the following relation for the total acceleration in TeVeS:

$$g_M(r) = g_N(r) + \sqrt{g_N(r)a_0}, \quad (17)$$

where $a_0 = 1.2 \times 10^{-10} \text{ms}^{-2}$. Exploiting the above and introducing $z_0 = (x \cos \phi - y \sin \phi) \tan \theta$, the deflection angle's x -component yields

$$\alpha_x = 2(x - b \cos \phi \cos \theta) \int_{-\infty}^{z_0} \frac{dz}{r'} \left(\frac{GM}{(r' + h)^2} + \frac{\sqrt{GMa_0}}{r' + h} \right) + 2(x + b \cos \phi \cos \theta) \int_{z_0}^{\infty} \frac{dz}{r'} \left(\frac{GM}{(r' + h)^2} + \frac{\sqrt{GMa_0}}{r' + h} \right). \quad (18)$$

The integral (18) can be evaluated by means of elementary calculus, but as the resulting expression is quite lengthy, we shall skip its presentation at this point. Analogously, the closed analytic form

for α_γ can be derived, and as a consequence, this is also true for the lensing quantities κ and γ .

2.3 Cosmology and distances

Concerning the calculation of distances in gravitational lensing, we shall adopt a standard flat Λ CDM cosmology with $\Omega_m = 0.3$ and $\Omega_\Lambda = 0.7$. This choice is justified by the fact that many covariant formulations of MOND mimic the behavior of a Λ CDM, accounting for marginal differences that will have no significant impact on our analysis. For instance, Zhao et al. (2006) presented a minimal-matter open model with a cosmological constant which works to good accuracy for redshifts $z \lesssim 3$. Furthermore, Angus et al. (2007b) proposed the flat μ HDM cosmological model based on the assumption of massive (sterile) neutrinos. If provided with a cosmological constant, this model is quite similar to the standard flat Λ CDM model, being capable of explaining the cosmic microwave background (Skordis et al. 2006). Recent work has also shown that it seems possible to construct certain covariant formulations of MOND giving a cosmology identical to Λ CDM in the matter-dominated era (Zhao 2007).

3 FITTING PROCEDURE

We will follow Kayser (1990) to model the lens systems: For each pair of images i and j , when tracing one light-ray back for each observed image to the source plane, the source position obtained from Eq. (10) should be the same for both images. We can thus simply compare the resulting source position for each image by computing their squared deviation,

$$\Delta_s^2 = \sum_{i \neq j} \left((x_{si} - x_{sj})^2 + (y_{si} - y_{sj})^2 \right), \quad (19)$$

where x_s and y_s is the source position in Eq. (10). This is a measurement of how well the images retrace back to a single point in the source plane.

Another quantity to minimize is the deviation of the lens center from the observed optical center, given by

$$\Delta_l^2 = \left((x_l)^2 + (y_l)^2 \right), \quad (20)$$

However, our model has generally 9 fitting parameters (the lens mass M , the Kuzmin length b , the Hernquist length h , the PA angle, the inclination i , the source position x_s, y_s , and the lens position x_l, y_l), while for a double-imaged system we have only four constraints from the two image positions, and another two constraints from the observed lens optical center. The problem is thus ill-posed.

To cure this, and ensure the uniqueness of the solution, we use a regularization method by adding a regularization term in the minimization. This term is penalizing solutions deviating from the fundamental plane as well as face-on¹ and disky solutions, and solu-

tions with an anomalous mass-to-light ratio or a large flux anomaly:

$$\mathcal{P} = \left[(\log FP)^2 + (\cos i)^2 + \left(\frac{b}{b+h} \right)^2 \right] + \left[\log \frac{f_{AB}}{f_{\text{obs}}} \right]^2 + \left[\log \frac{M}{M_{\text{stellar}}} \right]^2. \quad (21)$$

The deviation from the fundamental plane is measured by $\log FP = \log(h/h_1) - 1.26 \log(M/M_1)$, and $h_1 = 0.72 \text{kpc}$ and $M_1 = 1.5 \times 10^{11} M_\odot$ (Chen & Zhao 2006).

We choose a very small regularization parameter $\lambda \sim (0.003'')^2$, and minimize the following regularized “ χ^2 -like” quantity,

$$\eta^2 = \Delta_s^2 + \Delta_l^2 + \lambda \mathcal{P}, \quad (22)$$

for 14 double-imaged systems and four quadruple-imaged systems in the CfA-Arizona Space Telescope Lens Survey (CASTLES). Note that we also check that our results are insensitive to the detailed choice of the regularization parameter² and that, due to the sufficient amount of constraints (position of lens and images), the fitting procedure for quadruple-image lenses is performed with $\lambda = 0$. The results are shown in Table 1 and Table 2, respectively. Finally, note that the observed mass of each lens was calculated according to Sect. 7.1 of Zhao et al. (2006, Eqs. (73)-(75)).

4 FITTING RESULTS

4.1 Double-imaged systems

Setting $\Delta_s < 0.01''$ as a reasonable threshold for acceptable fits of the HK lens, Table 1 shows that our model is able to describe the observed image positions of all double-imaged systems, with quite a number of these systems yielding plausible parameters within the context of MOND/TeV s . Additionally, the HK model seems to be able to explain the flux ratios of these binaries in almost every case.

However, there are a few outliers which we will discuss in the following. Since the model should be capable of reproducing all observational constraints and the lens mass should have a value close to the stellar mass ($M/M_* \simeq 1$) in MOND/TeV s , these are characterized by very poor fitting parameters in terms of large differences between predicted and observed flux ratios and/or anomalous mass ratios M/M_* (deviation larger than a factor of 3).

4.1.1 RXJ0921+4529

The system RXJ0921+4529 contains two $z_s = 1.66$ quasars and a $H = 18.2$ spiral galaxy located in between the quasar images. According to Muñoz et al. (2001), this galaxy lens is quite likely to be a member of a $z_l = 0.32$ X-ray cluster centered on the observed field. Clearly, RXJ0921+4529 does not correspond to an isolated system, which complicates the situation in TeV s and provides a possible explanation for the extremely poor fit/mass ratio ($M/M_* \approx 59$). The presence of a cluster could have caused difficulties in fitting the lens as the impact of non-linear effects may

¹ As there is strong observational evidence supporting that the system B0218+357 corresponds to a nearly face-on spiral galaxy (e.g. Grundahl & Hjorth 1995; York et al. 2005), we choose the regularization term for this particular lens such that edge-on solutions are penalized instead. Further relaxing the penalties w.r.t. the fundamental plane and the observed flux ratio in Eq. (21), the fit substantially improves, corresponding to a factor of 20 in Δ_s .

² In case of RXJ0921+4529, however, our choice of λ creates an over-regularization effect, which results in a best-fit lens mass that is roughly by a factor 10 smaller than estimated by Zhao et al. (2006) fitting the system’s Einstein ring size. Decreasing the regularization parameter to $\lambda \sim (3 \times 10^{-4}'')^2$ is able to resolve this issue, with Δ_s dropping by a factor 10 and the lens mass now being in accordance with the previous estimate of Zhao et al. (2006) (see Table 1).

Table 1. Fitting results for selected 2-image lens systems from the CASTLES sample: In the table, the observed lens mass M_* is calculated according to Sect. 7.1 of Zhao et al. (2006, Eqs. (73)-(75)), the parameter r_h is the Hernquist length expected from half-light measurements (values are taken from Zhao et al. 2006). We do not give η^2 , but instead we list Δ_s and compare the inferred values of PA, the Hernquist length h , mass and flux ratio to observations. Additionally, we predict inclination and time delay for the particular lens models. Outliers are characterized by large differences between predicted and observed flux ratios and/or anomalous mass ratios M/M_* (deviation larger than a factor of 3) like, for instance, in case of RXJ0921+4529 which resides in a cluster. Note that the fitted lens position is given by $(x_l, y_l) \approx (0, 0)$ for all lenses.

Lens	z_l	b/h	h/r_h	M(fit/obs)	PA	incli.	Δ_s	$f_{AB}(\text{fit}/\text{obs})$	$\delta t(\text{fit}/\text{obs})$
			kpc	$10^{11} M_\odot$	degree	degree	arcsec	days	
Q0142-100	0.49	0.25	1.34/1.6	1.70/4.08	72.2	90.0	2.43×10^{-4}	8.06/8.22	151.5/-
B0218+357	0.68	1.0	2.19/1.8	2.69/2.67	-22.6	6.94	7.75×10^{-5}	0.759/0.587	7.52/10.5
HE0512-3329	0.93	0.24	1.45/1.8	1.49/2.91 ^a	28.2	90.0	3.90×10^{-6}	0.0013/1.175	19.6/-
SDSS0903+5028	0.39	0.76	1.83/1.8	2.77/3.80	-30.4	90.0	9.90×10^{-4}	2.29/2.17	135.2/-
RXJ0921+4529	0.31	0.037	7.59/1.8	20.0/0.34	60.2	90.0	5.85×10^{-4}	3.623/3.591	167.2/-
FBQ0951+2635	0.24	0.13	1.20/0.32	0.47/0.31	60.3	90.0	1.23×10^{-4}	2.74/3.53	13.2/-
BRI0952-0115	0.41	0.055	2.20/0.29	0.58/0.27	124.1	90.0	5.04×10^{-4}	3.52/3.52	8.11/-
Q0957+561	0.36	1.55	1.21/5.23	6.94/8.44	40.0	90.0	1.97×10^{-3}	14.3/1.08	752.4/417.0
Q1017-207	0.78	0.0092	2.39/1.19	0.83/0.74	88.8	89.9	2.16×10^{-4}	0.73/0.72	29.0/-
B1030+071	0.60	0.10	0.84/1.50	1.85/1.66	29.3	90.0	8.04×10^{-5}	36.6/36.6	346.8/-
HE1104-1805	0.73	0.33	0.58/2.48	4.91/3.32	61.9	90.0	1.96×10^{-3}	0.35/3.85	321.2/-
B1600+434	0.41	0.18	1.64/1.8	1.01/0.40	36.8	90.0	2.09×10^{-4}	0.83/0.84	32.2/51.0
PKS1830-211	0.89	0.48	2.75/1.8	1.33/1.48	62.3	90.0	4.14×10^{-4}	157.3/157.3	32.7/26.0
HE2149-2745	0.50	0.026	0.94/11.4	1.04/2.00	-30.0	90.0	2.30×10^{-4}	6.53/4.19	90.7/103.0
SBS0909+523	0.83	0.19	3.02/1.8	2.92/13.5 ^a	49.2	90.0	1.84×10^{-3}	1.42/1.42	65.9/-

^a Note that Zhao et al. (2006) used a different value for M_* based on a wrong magnitude in an older version of the CASTLES data set.

be important. In addition, note that there are still some unresolved issues in MOND/TeV s concerning clusters (e.g. Sanders 1999, 2003, 2007; Angus et al. 2007b; Feix et al. 2008).

4.1.2 Q0957+561

The gravitational lens Q0957+561 is the most thoroughly studied one in literature. The system involves a radio-loud quasar at redshift $z_s = 1.41$ which is mapped into two images by a brightest cluster galaxy (BCG) and its parent cluster at redshift $z_l = 0.36$ (e.g. Keeton et al. 2000; Barkana et al. 1999, and references therein). It is also known that the lens galaxy has a small ellipticity gradient and isophote twist which are properties the simple HK model cannot account for. Together with the fact that the lens is embedded into a cluster, this might be a reason for the huge discrepancy between observed and predicted flux ratio in the context of modified gravity.

4.1.3 HE1104-1805

The lens galaxy's colors are in agreement with a high-redshift early-type galaxy, and its redshift is roughly estimated as $z_l = 0.77$ (Lehár et al. 2000, and references therein). Concerning its lensing properties, the system HE 1104-1805 is quite uncommon in a sense that the lens is closer the bright image, rather than the faint one. As is known from lensing within the standard GR/CDM paradigm, simple models can create such configurations only for a narrow range of parameters due to the peculiar flux ratio. Assuming simple ellipsoidal lens models, however, these parameters imply a large misalignment between the light and the projected density. The only possibility to align the mass with the light is to have a shear field being approximately twice as strong as estimated from the particular lens model.

Furthermore, the observed image separation is by a factor 2–3

larger than that of a typical lens, strongly suggesting that the separation is enhanced by the presence of a group or a cluster. So far, however, there has been no direct observational evidence for such a structure in the lens' surrounding area.

Analog to the above-mentioned lens systems, the unsatisfying fit and the correspondingly inferred flux ratio might be a result of both lens environment and model limitations (see also Sect. 4.3 and 4.4).

4.1.4 SBS0909+523

SBS0909+523 shows two images of background quasar source at $z_s = 1.377$ separated by $1.11''$ (e.g. Lehár et al. 2000, and references therein). Optical and infrared HST images indicate that the lensing galaxy has a large effective radius and a correspondingly low surface brightness. Additionally, the lens galaxy's redshift is estimated as $z_l = 0.83$ (Lubin et al. 2000), and its total magnitude in the H -band has been measured as $H = 16.75 \pm 0.74$. Although the lens galaxy's colors are poorly measured, they seem consistent with those of an early-type galaxy at the observed redshift.

The large uncertainties are a result of the difficulty in subtracting the close pair of quasar images (Lehár et al. 2000). For instance, the uncertainty in the I -band magnitude, $I = 18.85 \pm 0.45$, allows for a deviation of the mass estimate M_* by a factor of roughly 2.3 on a 2σ level, where we have again used Eqs. (73)-(74) of Zhao et al. (2006). Thus, we argue that the low mass ratio (listed in Table 1) may be entirely due to these uncertainties in observed magnitudes, with better constrained observations possibly softening the problem in MOND/TeV s .

4.1.5 HE0512-3329

The system HE0512-3329 was discovered as a gravitational lens candidate in the course of a snapshot survey with the Space Telescope Imaging Spectrograph (STIS), with the images of the quasar

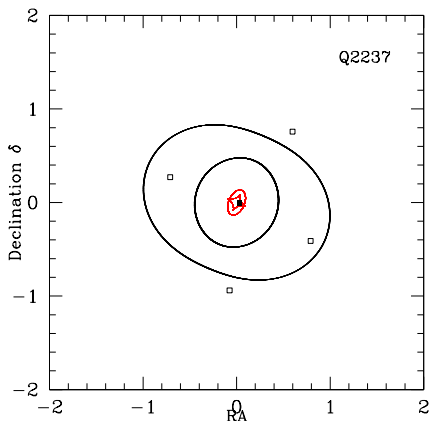


Figure 2. Critical curves (black) and caustics (red) of the best-fit Hernquist-Kuzmin model for Q2237+030: The empty and filled squares denote the observed positions of images and source, respectively.

source being separated by $0.644''$ (Wucknitz et al. 2003, and references therein). Although the lensing galaxy has not been detected yet, measurements of strong metal absorption lines at redshift $z = 0.93$, identified in the integrated spectrum, hint towards a damped Ly α system intervening at this redshift.

Analyzing separate spectra of both image components, Wucknitz et al. (2003) point out that both differential extinction and microlensing effects significantly contribute to the spectral differences and that one cannot be analyzed without taking into account the other. For lens modeling purposes, the observed flux ratio can therefore only be used after correcting for both effects. Thus, the large discrepancy between predicted and observed flux ratio might be a consequence of neglecting the above mentioned effects, rather than being intrinsic to MOND/TeVS.

4.2 Quadruple-imaged systems

As we can see from Table 2, most of the quadruple-imaged systems are very poorly fitted by our analytic HK lens model for MOND. In accordance with our goodness-of-fit criterion ($\Delta_s < 0.01''$) introduced in Sect. 4.1, there is just one system where the model is able to predict the image positions in a satisfying manner. Additionally, none of the observed flux ratios can be explained.

The only acceptable fit is given for Q2237+030, the nearby Einstein cross ($z_l = 0.04$; Huchra et al. 1985), which is the only true bulge-disk system in our set. Also, its physical Einstein ring size in the lens plane is very small, $R_E \approx 0.7\text{kpc}$ (in B1422+231, for instance, it is already by a factor of roughly 10 larger; Rusin et al. 2003). Nevertheless, it is not possible to give a reasonable explanation for the flux ratios using our smooth MOND lens model. Taking effects due to microlensing into account, which are not considered in this work, could be able to relax the situation. Note that the lens galaxy actually contains a bar feature (Yee 1988) which is ignored in our analysis.

4.2.1 PG1115+080

The lens galaxy in PG1115+080 and its three neighbors belong to a single group at $z_l = 0.311$, with the group being centered southwest of the lens galaxy's position (Kundic et al. 1997; Impey et al. 1998, and references therein). Reasonable fits of this lens typically

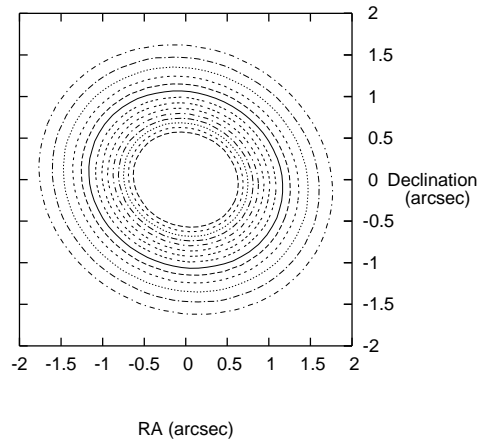


Figure 3. Convergence map κ of the best-fit Hernquist-Kuzmin model for Q2237+030, with the outer contour level being at $\kappa = 0.7$ and increasing in steps of 0.1 up to a level of $\kappa = 2.0$.

involve a significant amount of external shear in the context of GR/CDM. Moreover, the observed anomaly of the flux ratio (~ 0.9) between two of the images strongly hints towards an additional perturbation of the system caused by a satellite galaxy or a globular cluster. Similar to Sect. 4.1, we have a gravitationally bound system which will involve a more complicated approach in TeVeS than provided by the isolated HK model.

4.2.2 B1422+231

The system B1422+231 shows almost the same characteristics as PG1115+080 (Kundic et al. 1997, and references therein). Again, the lens belongs to a galaxy group which is centered south of the lens galaxy ($z_l = 3.62$). Kormann et al. (1994a) were able to fit the lensing system using a very flat singular isothermal ellipsoid (SIE; Kassiola & Kovner 1993; Kormann et al. 1994b) plus an external shear field. However, HST observations revealed that the lens galaxy's optical axis ratio is much closer to unity than assumed for the flat SIE, favoring rounder lens models with larger external shear.

4.2.3 SDSS0924+0219

Estimated colors and magnitudes of the lens galaxy are consistent with those of a typical elliptical galaxy at $z_l = 0.4$ (Inada et al. 2003, and references therein). Although the lens environment does not show any nearby objects perturbing the system, quite an amount of external shear is needed to obtain a satisfying fit to observations, with the lens being typically modeled by a (flattened) singular isothermal sphere (SIS). Additionally, microlensing plays an important role in explaining the observed flux ratios within GR/CDM, which is likely to be true in TeVeS as well.

4.3 Maximum non-spherical shear of a Kuzmin lens

As we have seen, the outliers in our selection of quadruple-image lenses correspond to systems with a large external shear. In PG1115+080, for example, this is due to a neighboring galaxy group. However, the same situation also appears in uncrowded environments, usually constraining the lensing potential to require a substantial ellipticity. From Sect. 4.2, it seems that our present

Table 2. Fitting results for selected 4-image lens systems from the CASTLES sample: Note that all positions (RA and declination) are given in units of arcsec. The observed position angle and inclination of Q2237+030 (major-axis) are PA= 77.2° and $i = 64.5^\circ$, respectively, assuming a circular face-on disk. Replacing the auxiliary Hernquist with a Jaffe profile barely changes the numbers: inclination and PA change by about 5 degrees, the predicted mass by roughly 10%.

	PG1115+080	Q2237+030	B1422+231	SDSS0924+0219
z_l	0.31	0.04	0.34	0.39
z_s	1.72	1.69	3.62	1.52
D_l (kpc)	957.2	163.6	1020.2	1116.6
D_s (kpc)	1874.2	1874.0	1637.6	1867.0
D_{ls} (kpc)	1413.2	1810.8	1341.7	1252.1
Image A	(-0.947, -0.690) ± 0.003	(-0.075, -0.939) ± 0.003	(0.375, 0.973) ± 0.003	(-0.162, 0.847) ± 0.003
Image B	(-1.096, -0.232) ± 0.003	(0.598, 0.758) ± 0.003	(0.760, 0.656) ± 0.003	(-0.213, -0.944) ± 0.003
Image C	(0.722, -0.617) ± 0.003	(-0.710, 0.271) ± 0.003	(1.097, -0.095) ± 0.003	(0.823, 0.182) ± 0.003
Image D	(0.381, 1.344) ± 0.003	(0.791, -0.411) ± 0.003	(-1.087, -0.047) ± 0.003	(-0.701, 0.388) ± 0.003
Source	(-0.011, 0.091)	(0.027, -0.0051)	(0.089, 0.030)	(-0.024, -0.047)
Lens	(-0.0011, -0.0041)	(0.00066, 0.00096)	(-0.00093, 0.0065)	(0.019, -0.0051)
M (M_{fit}/M_*) ($\times 10^{11} M_\odot$)	7.80/1.23	0.78/1.19	4.83/0.77	2.80/0.32
h (kpc)	2.25	0.44	8.42	1.57
b/h	0.56	1.85	0.29	2.17
PA angle (degree)	244.8	246.6	117.9	266.4
Inclination (degree)	44.5	30.6	48.6	40.5
Δ_s (arcsec)	0.0402	0.0026	0.0593	0.0612
Flux ratio(obs)	4.03:2.53:0.65:1	2.62:1.64:1.30:1	31.1:34.6:18.4:1	12.5:5.68:4.81:1
Flux ratio(fit)	3.98:4.15:1.40:1	0.81:0.66:0.68:1	8.56:6.53:7.51:1	1.66:0.69:0.86:1

analytic model is not able to generate such a potential in most cases. As is known, almost all quadruple-imaged systems show evidence for the need of an external shear field (Witt & Mao 1997; Kassiola & Kovner 1993; Keeton et al. 1997) by violating a certain inequality of the image positions. It is perhaps not surprising that the current isolated HK model fails to fit these lenses³.

To gain a better understanding about this issue, we consider a pure edge-on Kuzmin lens ($h = 0$) and derive the maximum variation of the shear at the Einstein radius R_E by comparing its values on the major and minor axis. For this reason, let us introduce a quantity Q being given as follows:

$$Q = \frac{\gamma(R_E, 0) - \gamma(0, R_E)}{\gamma(R_E, 0) + \gamma(0, R_E)}. \quad (23)$$

The parameter defined above will indicate the level of the shear field's non-sphericity at the Einstein radius and is a function of the dimensionless radius R_E/b . Note that, in case of the Kuzmin lens, the quantity Q depends on redshift.

Figure 4 shows Q as function of R_E/b for the pure Kuzmin model (solid line), assuming $a_0 D/c^2 = 0.03$. This value has been chosen in accordance with the majority of lens redshifts in the CASTLES sample, and changing it does have no significant qualitative impact on the basic outcome. Additionally, we also present the result for the SIE model (Kormann et al. 1994b), with the potential axis ratio varying from 0.7 to 0.9 (shown by horizontal lines). As we can see, the Kuzmin model becomes comparable to a very round SIE if $R_E/b \gtrsim 10$.

To obtain a sufficiently strong quadruple moment/non-spherical shear at the Einstein radius ($Q > 0.2$), these disk-only models must satisfy the condition $b > 0.2R_E$. In case of PG1115, the observed ring size can be estimated as $R_E \approx 5$ kpc, so to fit four images, one might actually expect that $b \gtrsim 1$ kpc. However, trying

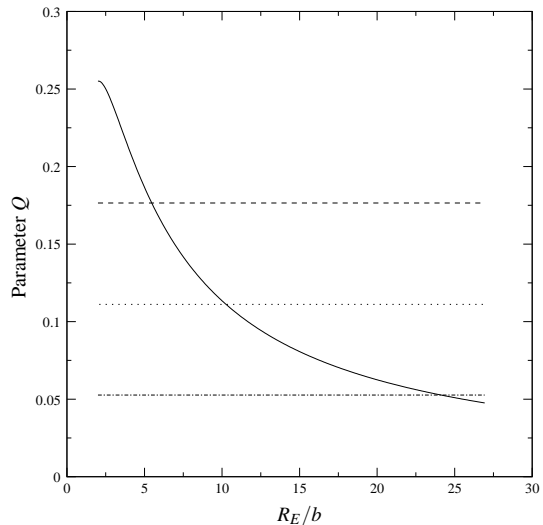


Figure 4. Non-spherical shear parameter Q for a simple TeVeS Kuzmin lens (solid line), assuming $a_0 D/c^2 = 0.03$. Additionally, we show the results for a SIE model with a potential axis ratio of 0.9 (dotted-dashed line), 0.8 (dotted line) and 0.7 (dashed line), respectively.

to fit the above mentioned Einstein ring size, using the stellar mass only, we also find that this would need a Kuzmin parameter close to zero ($b \approx 0$), corresponding to a very concentrated point-like lens. Although we have only given a plausibility argument, rather than a rigorous proof, this could explain why we cannot find a value of b that meets both requirements and why the HK model mostly fails to fit quadruple-imaged systems.

4.4 Experimenting with hypothetical lenses

Another possibility of investigating the fitting capability of our model is to generally explore its parameter space and to study the structure of critical curves and caustics. To avoid any limitations that might be due to the particularly chosen radial profile, we fur-

³ Note that our analysis does not take into account external shear effects, which would complicate the relation between lens mapping and associated density distribution due to non-linearity in modified gravity. While the main task of this paper is to explore the capability of the HK model, such contributions should certainly be addressed in future work.

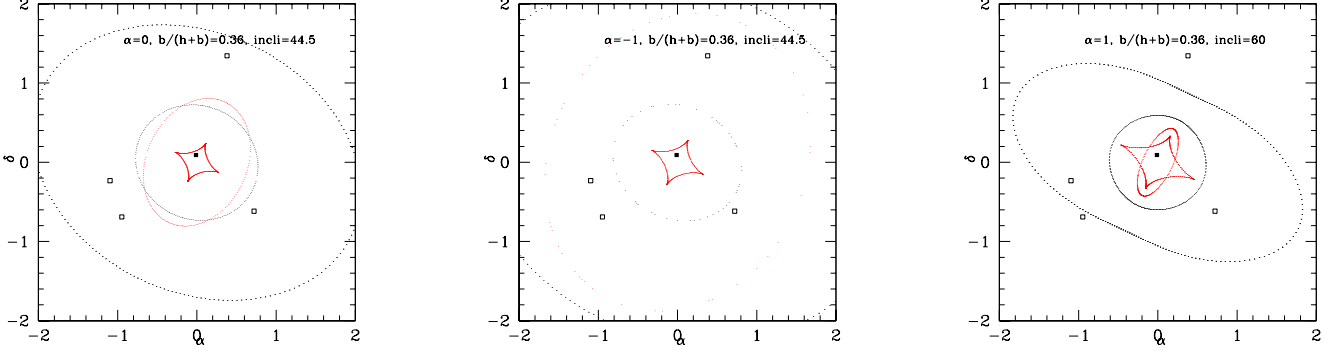


Figure 5. Experimenting with hypothetical lenses: Shown are the critical curves (black) and caustics (red) of different Dehnen-Kuzmin models characterized by the parameters α , $b/(h+b)$ and inclination (“core” radius and PA are fixed to $h = 0.72\text{kpc}$ and 77.2° , respectively). All models assume a lens mass of $M = 8 \times 10^{11} M_\odot$ which is approximately 8 times the stellar mass of the lens galaxy in PG1115+080. The empty and filled squares denote the observed image and source positions of PG1115+080.

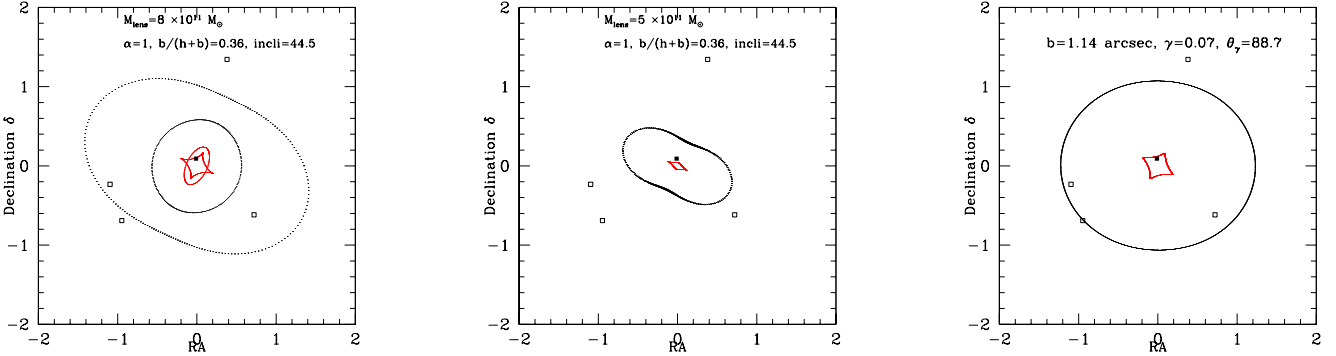


Figure 6. Effects of reducing the lens mass: Shown are the critical curves (black) and caustics (red) of a Dehnen-Kuzmin model ($\alpha = 1$, $b/(h+b) = 0.38$, $h = 0.72\text{kpc}$, PA = 77.2° and $i = 44.5^\circ$), assuming $M = 8 \times 10^{11} M_\odot$ (left panel) and $M = 5 \times 10^{11} M_\odot$ (middle panel), respectively. The empty and filled squares denote the observed image and source positions of PG1115+080, the stellar mass of the lens is estimated as $M_* \approx 10^{11} M_\odot$. Right panel: Critical curves (black) and caustics (red) of the best-fit $\text{SIS} + \gamma_{\text{ext}}$ model given by Eq. (25).

thermore replace the auxiliary Hernquist profile with the more general model proposed by Dehnen (1993). Its Newtonian potential and the corresponding density profile read as

$$\begin{aligned} \Phi_{N,D}(r) &= \frac{GM}{\alpha} \left[-1 + \left(\frac{r}{r+h} \right)^\alpha \right], \\ \rho_D(r) &= \frac{Mh(1+\alpha)}{4\pi r^{2-\alpha}(r+h)^{2+\alpha}}, \end{aligned} \quad (24)$$

where h is a characteristic length of the model. Depending on the value of α , the Dehnen model represents different density distributions, ranging from quite cuspy to more broadened profiles. For $\alpha = 0$ and $\alpha = 1$, Eq. (24) reduces to the models of Jaffe (Jaffe 1983) and Hernquist, respectively.

Allowing different values for α , we repeat the fitting procedure for the quadruple-imaged systems discussed in Sect. 4.2. The result is basically the same as for the HK model, with the parameters listed in Table 2 not significantly changing. In case of the Jaffe profile ($\alpha = 0$), for instance, inclination and PA are altered by about 5° and the predicted mass by approximately 10%.

To further illuminate this obvious insufficiency of our model, let us have a more detailed look at the caustic structure, taking the system PG1115+080 as an example: Choosing a plausible setting for the lens system in MOND, we fix its size to $h = 0.72\text{kpc}$ and the PA to 77.2° (observed value). In accordance with the best-fit

results, we additionally assume a lens mass of $M = 8 \times 10^{11} M_\odot$ and vary the Dehnen index α , the model’s “diskyness” $b/(h+b)$ as well as the inclination on a range from -1 to 1 , 0.1 to 0.9 and 10° to 90° , respectively. For a selection of such lenses, the corresponding critical curves and caustics are shown in Fig. 5. Then, among all resulting lens models, we select those which exhibit the strongest (non-spherical) shear, corresponding to a large astroid caustic size. Since the lens mass should be close to the stellar mass ($M/M_* \approx 1$) in MOND/TeVS, the idea is now to stepwise decrease the mass of these models. In all cases, we find that, due to the caustics’ contraction, the source crosses the astroid caustic way before M/M_* reaches unity, thus not corresponding to a quadruple-imaged system anymore. Typically, the crossing seems to take place when the lens model’s mass is roughly around $4 - 6 \times 10^{11} M_\odot$. For $\alpha = 1$, $b/(h+b) = 0.38$ and an inclination of 44.5° , this situation is illustrated in the left and middle panel of Fig. 6. Note that we have kept the source position fixed at $(-0.011, 0.091)''$ for our analysis, with the lens being centered at the origin.

Again, this provides a possible explanation why the Dehnen-Kuzmin model (including the HK model) mostly fails to fit quadruple-imaged systems, supporting our earlier conclusion from Sect. 4.3. Given that $M/M_* \approx 1$ in MOND, our model is obviously not able to generate sufficiently strong shear (hence large caustics) and a large Einstein ring at the same time. For comparison, we

also present the resulting caustics and critical curves of a best-fit $\text{SIS}+\gamma_{\text{ext}}$ model in the right panel of Fig. 6. As is known, its deflection potential can be expressed as

$$\Psi(\xi, \theta) = c\xi + \frac{\gamma}{2}\xi^2 \cos(2(\theta - \theta_\gamma)). \quad (25)$$

Choosing the lens' position $(x_l, y_l) = (0.0028, 0.0048)''$, $c = 1.14''$, $\gamma = 0.07$ and $\theta_\gamma = 88.7^\circ$, the above model is able to fit observations of PG1115+080 satisfyingly.

5 SUMMARY AND DISCUSSION

In this paper, we presented a class of analytic non-spherical models, called the Hernquist-Kuzmin models, that we applied to fit double-imaged and quadruple-imaged lens systems in the context of MOND, using the covariant framework of TeVeS. These analytic models interpolate smoothly between a Hernquist sphere and a Kuzmin disk, and their great advantage is that the solenoidal field of MOND, which normally appears in Eq. (1) for non-spherical configurations, is zero. Note that these models are not, *stricto sensu*, bulge-disk models (see Fig. 1).

After having worked out the lensing properties of the models, we devised a fitting procedure in order to fit 15 double-imaged systems and four quadruple-imaged systems in the CfA-Arizona Space Telescope Lens Survey (CASTLES). Since the fitting problem is ill-posed, especially in the case of double-imaged systems, we used a regularization method to ensure the uniqueness of the solution, by penalizing fits deviating from the fundamental plane as well as face-on and disky fits, and fits with an anomalous mass-to-light ratio or a large flux anomaly.

From this fitting procedure, we find that our model is able to describe the observed image positions of all analyzed double-imaged systems, and we can safely conclude that 10 of these systems yield plausible parameters within the context of MOND/TeVeS. Additionally, our analytic model is able to explain the flux ratios of these binaries in almost every case. One can thus conclude that, in general, galaxy lenses do not need dark matter in MOND/TeVeS. Note that the implied masses for most of these lenses are quite similar to those derived from the spherically symmetric models of Zhao et al. (2006), but that the big advantage of our non-spherical model is its ability to fit the precise image-positions rather than just the size of the Einstein ring.

On the other hand, 5 double-imaged systems do not provide a reasonable fit: while for two of these systems, the found problems are likely to be solved by considering observational uncertainties, a more accurate model and/or additional effects such as extinction and microlensing, the other three lenses appear to be lacking an obvious explanation⁴. It is however quite striking that all these remaining outliers are actually residing in (or close to) *groups or clusters* of galaxies. This means that non-linear effects could have an important incidence, since lensing in MOND is much more sensitive to the three-dimensional distribution of the lens (and of the environment) than in GR (e.g. Feix et al. 2008). Moreover, it is known for a while that additional dark matter is needed for clusters of galaxies in MOND (e.g. Sanders 1999, 2003, 2007; Angus et al. 2007b; Milgrom 2007), and it has recently been shown that this was

the case for groups, too (Angus et al. 2007a). Possible explanations for this “cluster dark matter” in the context of MOND range from the presence of numerous clouds of cold gas (Milgrom 2007) to the existence of sterile neutrinos with a 5eV mass (Gentile et al. 2007), through the non-trivial effects of the vector field (or of an additional scalar field) in covariant formulations of MOND other than TeVeS (e.g. Sanders 2005; Zhao 2007). In any case, many studies, including the recent analysis of the velocity dispersions of globular clusters in the halo of NGC 1399 (Richtler et al. 2007), have also provided evidence for such dark matter on *galaxy scales* in MOND: this is typical for galaxies residing at the center of clusters only, and can be interpreted (Richtler et al. 2007) as a small-scale variant of the aforementioned problem of MOND in clusters. This could thus provide an additional, physical, reason to the poor fits obtained here for the two-image lenses residing in groups or clusters.

For the four quadruple-imaged systems, it is a different story: the only acceptable fit is obtained for the Einstein cross Q2237+030, but even in this case, the observed flux ratios cannot be reproduced. However, the anomalous flux ratios here are most likely due to microlensing effects which have not been considered in our analysis. We can thus conclude that MOND does not provide a solution to the flux anomaly issue, mainly because smooth MOND models naturally predict smooth amplification patterns. Among the 3 very poorly fitted lenses, only PG1115+080 and B1422+231 appear in a crowded environment, which could cause the same perturbing effects as for non-isolated double-imaged systems; the remaining lens, SDSS0924+0219, appears relatively isolated.

We thus argue that, especially in this particular case, the poor fits are due to the intrinsic limitation of our analytic models: we indeed showed that our models were unable to produce a large Einstein ring and a large shear at the same time. Although we did not present a rigorous proof, we tried to make this limitation plausible by analyzing the maximum non-spherical shear of a TeVeS Kuzmin lens as well as the caustic structure of different Hernquist-Kuzmin models. To make the mass more concentrated, we also tried a Dehnen model (Dehnen 1993), but this did not provide a satisfactory solution either. Again, note that our analysis did not consider any contribution due to external shear effects.

We therefore conclude that our analytic models provide good MOND fits to the image positions of isolated two-image lenses, but that some problems are encountered for non-isolated two-image lenses. On the other hand, we showed that our models were barely able to fit quadruple-imaged systems. The present study has thus pinpointed some lenses for which a full three-dimensional numerical model should be devised in MOND. While these analytic models did obviously not yet represent a definitive test of MOND with gravitational lensing, they nevertheless provided a new step in understanding this quite unexplored research area, and in isolating the possibly challenging lensing systems for the future.

ACKNOWLEDGMENTS

HYS and BF acknowledge hospitality at the University of St Andrews. HYS thanks Prasenjit Saha and Muhammad Yusaf for valuable comments on an earlier version of the manuscript. BF is supported by the FNRS, HSZ acknowledges partial support from the Chinese National Science Foundation (Grant No. 10233040) and a UK PPARC Advanced Fellowship. MF is supported by a scholarship from the Scottish Universities Physics Alliance (SUPA). We

⁴ Note, however, that the stellar mass estimates depend on the adopted initial mass function and star formation rate, and can vary by a factor of 4 in the R-band, which could partly solve the problem of the mass-ratio discrepancy, but not the flux ratio anomalies.

thank the referee Bob Sanders for insightful comments and useful suggestions.

REFERENCES

- Angus, G. W., Famaey, B., & Buote, D. A. 2007a, ArXiv e-prints, 709
- Angus, G. W., Shan, H. Y., Zhao, H. S., & Famaey, B. 2007b, ApJ, 654, L13
- Barkana R., Lehár J., Falco E. E., Grogin N. A., Keeton C. R., Shapiro I. I., 1999, ApJ, 520, 479
- Bekenstein J., Milgrom M., 1984, ApJ, 286, 7
- Bekenstein J. D., 2004, Phys. Rev. D, 70, 083509
- Bekenstein J. D., 2006, Contemp. Phys., 47, 387
- Bruneton J.-P., Esposito-Farese G., 2007, ArXiv e-prints, 705
- Chen D.-M., Zhao H., 2006, ApJ, 650, L9
- Chiu M.-C., Ko C.-M., Tian Y., 2006, ApJ, 636, 565
- Ciotti L., Londrillo P., Nipoti C., 2006, ApJ, 640, 741
- Dehnen W., 1993, MNRAS, 265, 250
- Dodelson S., Liguori M., 2006, Physical Review Letters, 97, 231301
- Famaey, B., Angus, G. W., Gentile, G., & Zhao, H. S. 2007a, ArXiv e-prints, 706
- Famaey, B. & Binney, J. 2005, MNRAS, 363, 603
- Famaey, B., Bruneton, J.-P., & Zhao, H. 2007b, MNRAS, 377, L79
- Famaey, B., Gentile, G., Bruneton, J.-P., & Zhao, H. 2007c, Phys. Rev. D, 75, 063002
- Feix M., Fedeli C., Bartelmann M., 2008, A&A, 480, 313
- Gentile G., Zhao H. S., Famaey B., 2007, ArXiv e-prints, 712
- Grundahl F., Hjorth J., 1995, MNRAS, 275, L67
- Hernquist L., 1990, ApJ, 356, 359
- Huchra J., Gorenstein M., Kent S., Shapiro I., Smith G., Horine E., Perley R., 1985, AJ, 90, 691
- Impey C. D., Falco E. E., Kochanek C. S., Lehár J., McLeod B. A., Rix H.-W., Peng C. Y., Keeton C. R., 1998, ApJ, 509, 551
- Inada N., Becker R. H., Burles S., Castander F. J. et al., 2003, AJ, 126, 666
- Jaffe W., 1983, MNRAS, 202, 995
- Kassiola A., Kovner I., 1993, ApJ, 417, 450
- Kayser R., 1990, ApJ, 357, 309
- Keeton C. R., Falco E. E., Impey C. D., Kochanek C. S. et al., 2000, ApJ, 542, 74
- Keeton C. R., Kochanek C. S., Seljak U., 1997, ApJ, 482, 604
- Kormann R., Schneider P., Bartelmann M., 1994a, A&A, 286, 357
- Kormann R., Schneider P., Bartelmann M., 1994b, A&A, 284, 285
- Kundic T., Cohen J. G., Blandford R. D., Lubin L. M., 1997, AJ, 114, 507
- Kundic T., Hogg D. W., Blandford R. D., Cohen J. G., Lubin L. M., Larkin J. E., 1997, AJ, 114, 2276
- Kuzmin G., 1956, Astron. Zh., 33, 27
- Lehár J., Falco E. E., Kochanek C. S., McLeod B. A. et al., 2000, ApJ, 536, 584
- Lubin L. M., Fassnacht C. D., Readhead A. C. S., Blandford R. D., Kundić T., 2000, AJ, 119, 451
- McGaugh S. S., de Blok W. J. G., Schombert J. M., Kuzio de Naray R., Kim J. H., 2007, ApJ, 659, 149
- Milgrom M., 1983, ApJ, 270, 365
- Milgrom M., 2007, ArXiv e-prints, 712
- Miyamoto M., Nagai R., 1975, PASJ, 27, 533
- Muñoz J. A., Falco E. E., Kochanek C. S., Lehár J. et al., 2001, ApJ, 546, 769
- Qin B., Wu X. P., Zou Z. L., 1995, A&A, 296, 264
- Richtler T., Schubert Y., Hilker M., Dirsch B., Bassino L., Romanowsky A. J., 2007, ArXiv e-prints, 711
- Rusin D., Kochanek C. S., Keeton C. R., 2003, ApJ, 595, 29
- Sanders R. H., 1999, ApJ, 512, L23
- Sanders R. H., 2003, MNRAS, 342, 901
- Sanders R. H., 2005, MNRAS, 363, 459
- Sanders R. H., 2007, MNRAS, 380, 331
- Sanders R. H., McGaugh S. S., 2002, ARA&A, 40, 263
- Schmidt F., Liguori M., Dodelson S., 2007, Phys. Rev. D, 76, 083518
- Schneider P., Ehlers J., Falco E. E., 1992, Gravitational Lenses. Gravitational Lenses, XIV, 560 pp. 112 figs.. Springer-Verlag Berlin Heidelberg New York. Also Astronomy and Astrophysics Library
- Skordis C., 2008, ArXiv e-prints, 801
- Skordis C., Mota D. F., Ferreira P. G., Bøhm C., 2006, Physical Review Letters, 96, 011301
- Takahashi R., Chiba T., 2007, ApJ, 671, 45
- Tiret O., Combes F., 2007, A&A, 464, 517
- Witt H. J., Mao S., 1997, MNRAS, 291, 211
- Wucknitz O., Wisotzki L., Lopez S., Gregg M. D., 2003, A&A, 405, 445
- Xu D., Feix M., Shan H., Famaey B., Limousin M., Zhao H., 2007, ArXiv e-prints, 710
- Yee H. K. C., 1988, AJ, 95, 1331
- York T., Jackson N., Browne I. W. A., Wucknitz O., Skelton J. E., 2005, MNRAS, 357, 124
- Zhang P., Liguori M., Bean R., Dodelson S., 2007, Physical Review Letters, 99, 141302
- Zhao H., 2007, ApJ, 671, L1
- Zhao H., Bacon D. J., Taylor A. N., Horne K., 2006, MNRAS, 368, 171
- Zlosnik T. G., Ferreira P. G., Starkman G. D., 2007, Phys. Rev. D, 75, 044017